

Effect of hybrid polymer coating of Bioglass[®] foams on mechanical response during tensile loading

L. Bertolla, Z. Chlup, L. Stratil, A. R. Boccaccini & I. Dlouhý

To cite this article: L. Bertolla, Z. Chlup, L. Stratil, A. R. Boccaccini & I. Dlouhý (2015) Effect of hybrid polymer coating of Bioglass[®] foams on mechanical response during tensile loading, *Advances in Applied Ceramics*, 114:sup1, S63-S69, DOI: [10.1179/1743676115Y.0000000041](https://doi.org/10.1179/1743676115Y.0000000041)

To link to this article: <http://dx.doi.org/10.1179/1743676115Y.0000000041>



© 2015 The Author(s). Published by Taylor & Francis.



Published online: 04 Jul 2015.



Submit your article to this journal [↗](#)



Article views: 207



View related articles [↗](#)



View Crossmark data [↗](#)

Effect of hybrid polymer coating of Bioglass[®] foams on mechanical response during tensile loading

L. Bertolla^{*1}, Z. Chlup¹, L. Stratil¹, A. R. Boccaccini² and I. Dlouhý¹

A simplified two-dimensional finite elements model was created for a polyvinyl alcohol (PVA) coated Bioglass[®] strut undergoing tensile stresses (loading mode I). The strengthening contributions due to the infiltration of coating into surface cracks and coating's stiffness were evaluated in terms of stress intensity factor K_I and tensile stresses σ_{yy} in the proximity of the crack tip. The infiltration of the coating until the crack tip resulted as the most effective criterion for the struts strengthening. Bioglass[®] based scaffolds were dip coated into PVA and PVA/microfibrillated cellulose (MFC) aqueous solutions and tested in tensile load. Coated samples exhibited remarkably higher tensile strength than non-coated ones, which further raised with the increased amount of MFC. Contact angle θ and linear viscosity η measurements of PVA/MFC solutions showed that MFC caused a reduction in θ and a drastic increase in η , indicating that a balance between these two effects must be achieved.

Keywords: Bioceramics, Bioglass[®] scaffolds, Polymer coating, Composite coating, Mechanical properties, Cellulose, Tensile strength

This paper is part of a special issue on glass and ceramic composites for high technology applications (GlaCERCo)

Introduction

Synthetic biodegradable polymer coatings have been considered in several works as a reinforcing element for brittle bioactive glass scaffolds.^{1–3} By taking into account the stress–strain curves of polymer coated ceramic scaffolds obtained either from compressive or tensile tests, two different contributions to strengthening can be detected. The first one can be identified as a remarkable increase in the stress value at which the first fracture event occurs in comparison with non-coated samples. This behaviour could be ascribed to a lowering of the stress concentration at the defect sites on the strut surface, which allows a further increase in the remote load without any failure occurs.⁴ As far as the authors' knowledge is concerned, no computational evidence to validate such hypothesis can be found in the literature. The second effect is a stable damage process beyond the peak stress, commonly referred as 'plateau region'. The extent of the plateau region has been reported as depending on the mechanical properties of the coating material itself (i.e. Young's modulus, strength and strain to failure).⁴ From this standpoint, the adhesion between coating and substrate plays a fundamental role since the external loads must be transferred from the struts to the coating through the interface.⁵ The aim of this work is to enlighten in which way the coating allows such

remarkable extension of the elastic domain. More specifically, the authors' interest is to assess, through computational methods, which factor among the stiffness of the coating material and the extent of coating infiltration into surface cracks is the most effective in terms of reduction of the stress concentration at defect sites. During the initial stage of loading, the stiffness of coating would affect the crack opening displacement for a given external load, whereas the extent of coating infiltration would cause stresses redistribution at the crack tip. For complex three-dimensional structures as scaffolds are, this kind of study would turn out into an extremely demanding task. Moreover, scaffolds produced by foam replication technique exhibit large amount of defects: pores, powder granules not fully consolidated, cavities and cracks deriving from cooling or burning out of polymeric template.⁶ Therefore, it is convenient to simplify the problem to an ideal case. For this purpose, a part representing a two-dimensional cracked strut has been created, and its elastic response to a mode I loading configuration has been simulated by finite element modelling (FEM). Two different studies respectively evaluating the influence of coating stiffness and coating infiltration on K_I and σ_{yy} were performed. In order to experimentally validate the latter aspect, the parameters that determine the infiltration of a polymeric solution on a specific glass surface (i.e. wettability and viscosity) can be measured and then correlated to the results obtained from mechanical testing of the corresponding polymer–scaffold system. Previous studies on dip coated plates have, for instance, shown that the thickness of deposited liquid film coatings depends on the precursor solution properties such as density, surface tension as well as withdrawal speed from

¹Institute of Physics of Materials, Academy of Sciences of the Czech Republic, Žitkova 22, Brno 61662, Czech Republic

²Institute of Biomaterials, Department of Materials Science and Engineering, University of Erlangen–Nuremberg, Erlangen 91058, Germany

*Corresponding author, email bertolla@ipm.cz

the coating solution.^{7,8} Moreover, the wettability of the polymer solution determines the adhesion of the resulting film on the interface.⁹ Besides a thermodynamic driving force, the viscosity of the polymeric solution plays also a role in the infiltration capability, which should be as low as possible in order to be able to infiltrate into the cracks and defect at greater extent.¹⁰ Since the previous investigations performed by the authors were focused on the reinforcement effect of polyvinyl alcohol (PVA) and PVA/microfibrillated cellulose (MFC) composite coatings on Bioglass® scaffolds,^{11,12} in the present work, the wettability of aqueous PVA and PVA/MFC solutions having increasing amount of fibres was measured on a 45S5 Bioglass® substrate. The final mechanical properties of polymer coated porous ceramics are additionally affected by other parameters related to the coating process itself such as the removal technique of the excess polymer, the concentration of the polymer solution, the atmospheric pressure, humidity, eventual heat treatment, a number of dipping, etc.^{14,15} Since the dip coating procedure described in this work was performed manually can be considered not subject to considerable speed variations, the parameters that were considered in the present study were the viscosity and contact angle.

Experimental

Commercially available bioactive glass powder [45S5 Bioglass® composition: 45SiO₂–24.5CaO–24.5Na₂O–6P₂O₅ (wt-%); Schott AG, Germany] having average particle size of 4 μm (d_{50} , 4.0 ± 1.0 μm; d_{95} , ≤20 μm) was used in this investigation. Fully hydrolysed PVA, $d = 1.269$ g cm⁻³ (Sigma Aldrich Chemie GmbH, Germany), and MFC gel, with 2 wt-% fibre content (Borregard AS, Norway), were used. The slurry and scaffolds were prepared according to the procedure reported in Ref. 16. The resulting scaffolds were parallelepipeds having sizes 5 × 10 × 20 mm. The remaining slurry was used for the production of bulk substrates and bars for measurements of contact angles and Young's modulus by resonance methods respectively. After being cast in cylindrical rubber mould, the green bodies were dried for 72 h at room temperature and then for 24 h in a ventilated oven at 60°C. Sintering was carried out by following the same thermal treatment used for scaffolds in order to obtain comparable microstructures. Both surfaces were then abraded in order to make them parallel and subsequently polished using diamond paste with a particle size up to 1 μm. Some of them were cut into bars having sizes of 3 × 2 × 30 mm. Archimedes' method was used to measure the density of bulk Bioglass®, using a digital balance having an accuracy of ±0.0001 g (Denver Instruments, USA) and distilled water as buoyant. For the production of coatings, 1 g PVA was dissolved into 50 mL of water at 90°C by vigorous stirring for 1 h. The MFC gel (corresponding to the desired amount of dry fibres) was then added to the PVA water solution. Following this procedure, three different batches were produced, containing 0, 5 and 10 wt-%MFC respectively. All the solutions were stirred for 2 h, sonicated for 30 min and stirred again for 3 h at room temperature. Scaffolds were soaked into the solutions for 5 min and manually retrieved. Samples were dried in a ventilated oven at 50°C for 24 h. Small amount of liquid was withdrawn from each batch and used for contact angle measurement. Scaffolds' porosities before coating

were calculated by means of geometrical weight–volume measurements as

$$P = \left(1 - \frac{\rho_s}{\rho_b}\right) \times 100 \quad (1)$$

where ρ_b is the density of the bulk Bioglass® (assumed 2.7 g cm⁻³),¹⁷ and ρ_s is the apparent density of the scaffold (weight/volume ratio). The porosity of coated samples was calculated by the modified relationship

$$P = \left(1 - \frac{\rho_s}{\rho_b} - \frac{\rho_{cm}}{\rho_{ct}}\right) \times 100 \quad (2)$$

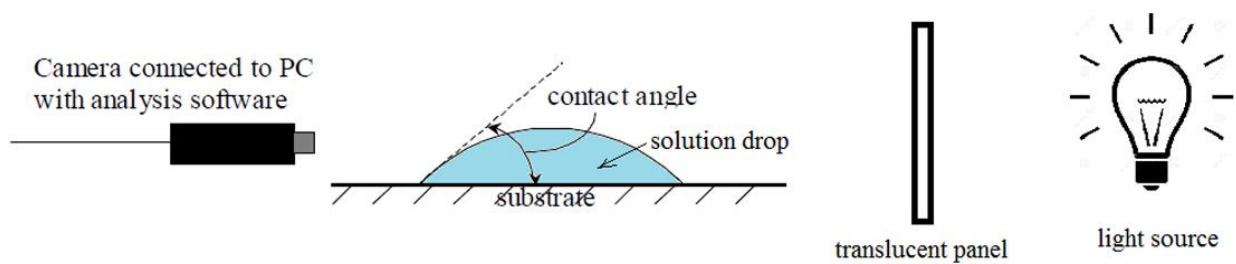
where ρ_{cm} is the coating density calculated for each sample as

$$\rho_{cm} = \frac{w_f - w_i}{V} \quad (3)$$

where w_i and w_f are respectively the weight of the scaffold before and after coating, and V is the scaffold's volume. ρ_{ct} is the theoretical coating density calculated by the mixture rule as

$$\rho_{ct} = X_{MFC}\rho_{MFC} + X_{PVA}\rho_{PVA} \quad (4)$$

where X_{MFC} and X_{PVA} are the mass fractions of MFC and PVA, and ρ_{MFC} and ρ_{PVA} are their densities respectively. The value of ρ_{MFC} is assumed equal to 1.14 g cm⁻³ from Ref. 18. The method for determining contact angles was as described in BS EN 828.¹⁹ Bioglass® substrates were placed underneath a syringe, and a drop of liquid was dispensed onto the substrate. The silhouette of the drop was viewed through a camera connected to a PC to capture video images of the drops. A light source was placed behind the drop in order to achieve better contrast. ImageJ analysis software was then used to measure the contact angle. The whole setup is schematised in Fig. 1. For each batch, three measurements were conducted, and the resulting values were averaged. Viscosimetry measurements were carried out by Discovery Hybrid Rheometer HR2 (TA Instrument), using a Peltier concentric cylinder temperature system with gap and rotor geometry. For tensile tests, a Z050 uniaxial screw driven load machine (Zwick GmbH, Germany) with 1 kN load cell was used applying a crosshead speed of 0.5 mm min⁻¹. Tensile strength values were determined dividing the maximum load recorded by the cross-sectional area of the specimen measured before the test. For each set, minimally six samples were tested, and average tensile strength values are reported. The surface topography of coated scaffolds was investigated by a scanning electron microscope (Lyra3, Tescan, Czech Republic; FEG-SEM Zeiss Ultra Plus, Germany). Abaqus 6.10 was used for FEM of a simplified two-dimensional cracked Bioglass® strut having rectangular shape and loaded in plane stress conditions. The Poisson's ratio for Bioglass® was set as $\nu_b = 0.26$.²¹ In order to measure the Young's modulus of Bioglass® E_b , bulk samples were prepared. The remainder of the slurry used for fabrication of scaffolds was cast in a cylindrical mould and kept drying for 7 days at room temperature. The Young's modulus of Bioglass® E_b was measured by the impulse resonance technique on rectangular samples using a commercial testing instrument (GrindoSonic: MK5 'Industrial', Belgium) and calculated using the experimentally determined resonant frequency, according to the standard ENV 843-2.²⁰ For FE analysis (FEA), the Young's modulus E_{PVA} and the Poisson's ratio of PVA ν_{PVA} were set as 4.1 GPa



1 Set-up used for measurement of contact angles of PVA/water and PVA/water/MFC solutions

(Ref. 22) and 0.46 (Ref. 23) respectively. The strut width ($W = 1$ mm), strut height ($h = 2$ mm), crack length ($a = 0.5$ mm) and crack tip radius ($\rho = 0.003$ mm) were used. The width of the ligaments was defined as $b = W - a$. For all models, the displacement was driven in small deformation and elastic regime. The modelled strut part was loaded by displacement, being constrained at the lower side and undergoing a displacement $\Delta y = +0.00017$ mm along the Y direction on the top side. The stress intensity factor K_I was determined via contour integral with the option of no degeneracy of elements at the crack tip (crack tip elements were all hexagonal shape) and using the criterion of maximum tangential stress. For studying the influence of coating infiltration on K_I and σ_{yy} , five models were created: a non-coated strut, a strut with coating just on the surface and struts having respectively one-third, two-thirds and completely filled crack. For simplicity, the models are referred as 1, 2, 3, 4 and 5 respectively. Then, the influence of E_{PVA} on K_I was also evaluated. For this purpose, a strut having the same configuration as model 5 was considered, and four simulations with increasing values of E_{PVA} (3, 5, 6 and 7 GPa) were run. These models were named as 6, 7, 8 and 9 respectively. Such values of E_{PVA} were chosen according to the authors' previous investigation,¹² and they were meant to be representative of PVA and PVA/MFC composite films having increasing stiffness. The element type CPS4R, featuring a four-node bilinear plane stress quadrilateral with reduced integration and hourglass control, was chosen. The number of elements and nodes for each model ranged from 5020 to 5817 and from 5185 to 5999 respectively. The coating was assumed to be perfectly adhering on the strut, and no debonding was considered. For each model, the computed σ_{yy} values near the crack tip were compared to the stress singularity function²⁴

$$\sigma_{yy} = \frac{K_I}{(2\pi r)^{1/2}} \quad (5)$$

where r is the distance from the crack tip along the x -axis.

Results and discussion

Finite element modelling

The experimental values of density and Young's modulus of Bioglass® were found equal to 2.57 g cm^{-3} and 38 ± 1.45 GPa respectively. The latter is in good agreement with Ref. 25. From this, the value of E_b was set as 38 GPa for FEA. The results obtained from FEA are summarised in Table 1. The distance from the crack tip, in which the singularity function fits the computed σ_{yy} distribution, has been defined as r_v (Table 1), and it decreases as the depth of PVA infiltration increases. For model 1, assumed as the reference solution, K_I

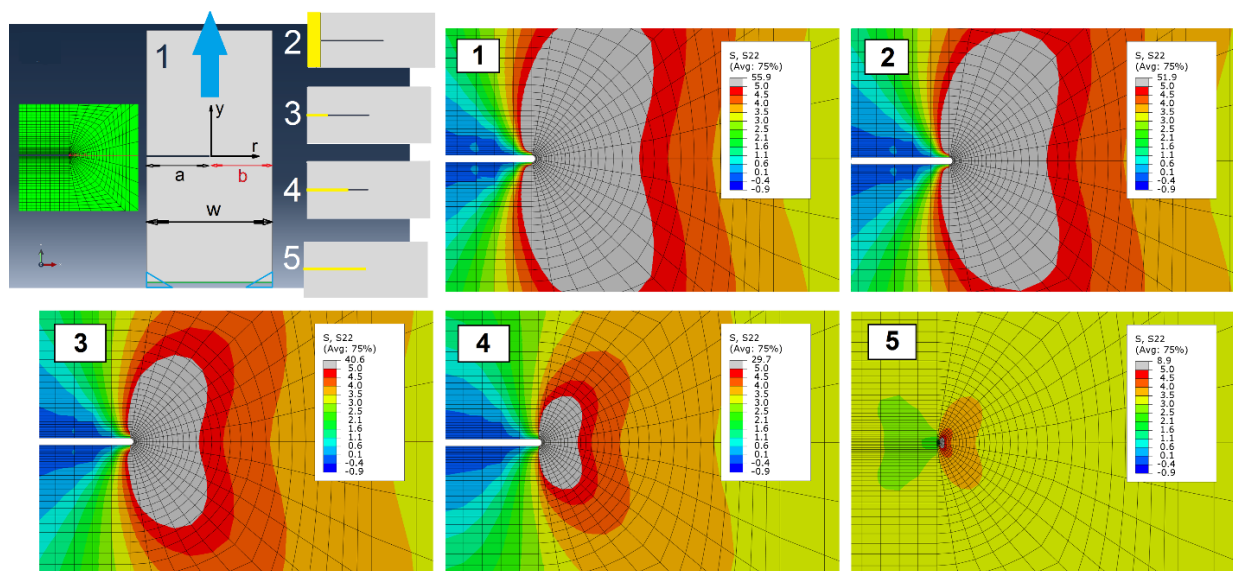
resulted as equal to $3.71 \text{ MPa m}^{1/2}$ and the computed σ_{yy} values were accurately fitted by equation (5) along the whole ligament width ($r_v = b$). For models 2–9, in which the crack geometry is modified by the presence of PVA, the stress fields at the crack tip are significantly influenced. It is interesting to point out that, for model 2, where no wetting of crack surfaces occurs, the reduction of K_I is almost negligible (5%) and $r_v \approx b$. As the PVA progressively penetrates into the crack, K_I and r_v decrease until reaching their minimum values ($K_I = 1.0 \text{ MPa m}^{1/2}$ and $r_v \approx 0.02b$) for model 5. In this case, the reduction of K_I in comparison with the reference model is 73%. The magnitude of σ_{yy} distribution near the crack tip decreases as well with the increasing infiltration depth, and it is shown in Fig. 2. In Table 1, σ_{yy} values at $r = 0.05$ mm ($\sigma_{yy|0.05}$) are compared for all the studied models. The variation of E_{PVA} (models 6–9) has only minor effect on σ_{yy} at the crack tip and thus on K_I . Therefore, the dominant criterion for the reduction of the stresses concentration near the crack tip is the extent of polymer infiltration inside the surface crack rather than the stiffness of the polymer itself.

Contact angle

The addition of MFC to an aqueous PVA solution caused a decrease in the contact angle. In previous studies, the influence of PVA concentration on the surface tension has been discussed.²⁶ Because of the presence of $-\text{OH}$ groups, PVA has the capability of H bonding with its solvents and decreases their surface tension as other surface active agents. In PVA aqueous solutions, both species, PVA (solute) and water molecules, are free to migrate and exert attractive forces of attraction on their immediate neighbours. Because of the difference in their structure and relative interaction with the neighbouring molecules in the solution, the fields of attractive forces exerted by the PVA molecules are different from those exerted by the water molecules. In the bulk solution, PVA molecules remain at a higher free energy state because of the large association tendency of water molecules among themselves through H bonds. Hence, PVA always has a tendency to migrate from bulk to the surface. The statistical accumulation in the surface of molecules with weaker fields results in a lowering of surface free energy.²⁶ In Fig. 3, the silhouettes of PVA, PVA/5%MFC and PVA/10%MFC of droplets on Bioglass® substrates are shown. Contact angle values are summarised in Table 2. Cellulose fibrils are also characterised by a high density of $-\text{OH}$ groups on the surface, which have the tendency to bond with adjacent $-\text{OH}$ groups by weak hydrogen bonding with other fibres, with PVA and water. Similarly for PVA,

Table 1 Description of FEM models (1–9) with related values of σ_{22} , K_I and r_v

Model	Description	E_{PVA}/GPa	$\sigma_{yy 0.05}/MPa$	$\sigma_{yy} \downarrow /%$	$K_I/MPa\ m^{1/2}$	$K_I \downarrow /%$	r_v/mm	r_v/b
1	Reference solution	4.1	19.62	...	3.71	0.0	0.500	1.00
2	PVA on the surface	4.1	18.14	7.5	3.54	4.6	0.500	1.00
3	1/3 filled crack	4.1	14.11	28.1	2.82	24.0	0.053	0.10
4	2/3 filled crack	4.1	10.38	47.1	2.13	42.6	0.035	0.07
5	3/3 filled crack	4.1	4.40	77.6	1.00	73.0	0.013	0.03
6	3/3 filled crack	3	4.74	75.8	1.07	71.2	0.014	0.03
7	3/3 filled crack	5	4.20	78.6	0.97	73.9	0.013	0.03
8	3/3 filled crack	6	4.04	79.4	0.94	74.7	0.012	0.03
9	3/3 filled crack	7	3.92	80.0	0.91	75.5	0.012	0.02



2 Two-dimensional part, mesh and models (1–5) used for FEM simulations with relative σ_{22} distribution



3 Drop profiles of a) PVA, b) PVA/5%MFC and c) PVA/10%MFC on Bioglass® substrates

Table 2 Summary of σ_t , P , θ and η and of tested scaffold and related coating solutions

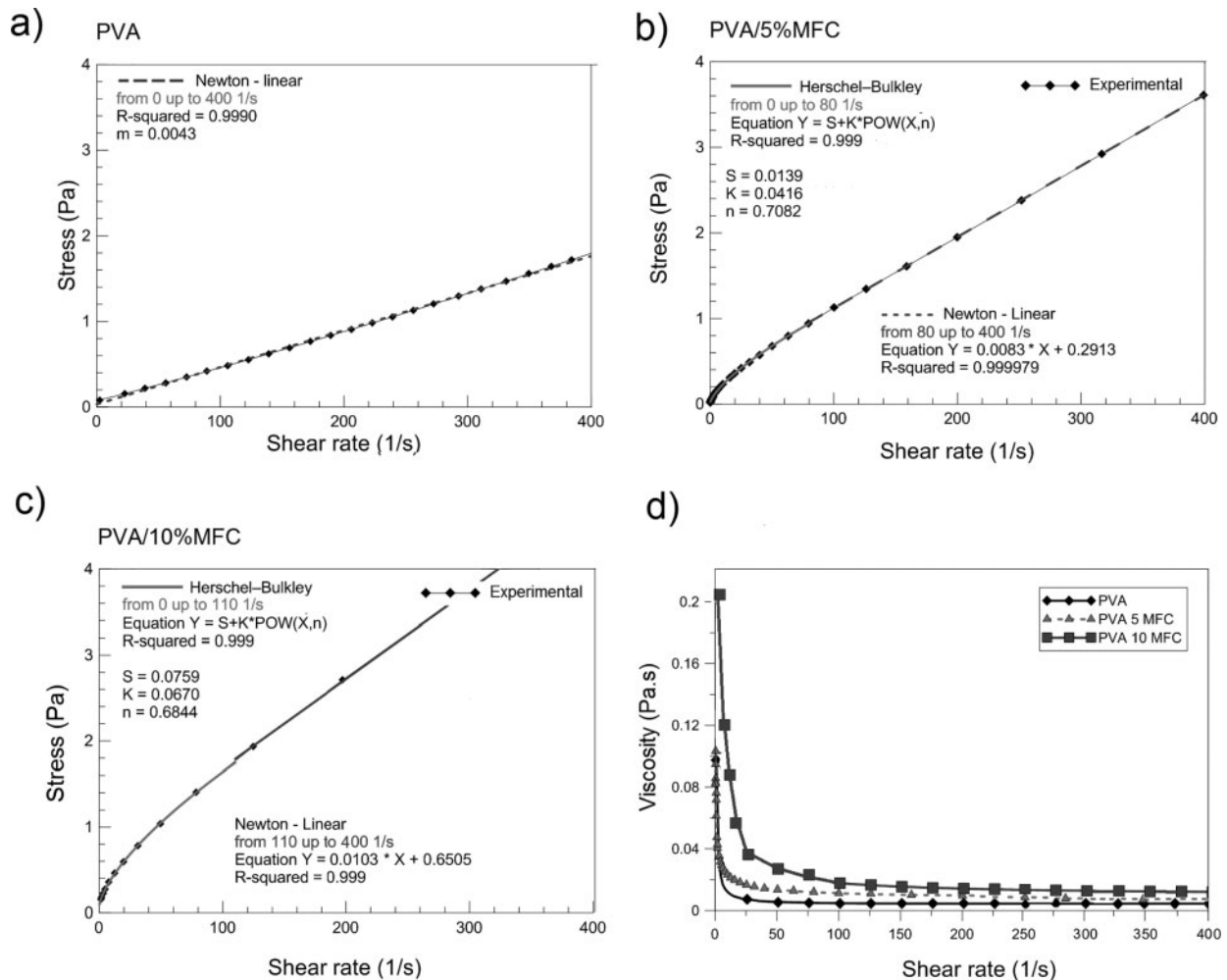
Coating	$P/%$	σ_t/MPa	$\theta/^\circ$	Linear $\eta/Pa\ s$
...	92.51	0.014 ± 0.0031
PVA	90.22 ± 0.56	0.196 ± 0.0090	45.14 ± 0.66	0.0043
PVA/5%MFC	90.38 ± 1.49	0.271 ± 0.0120	34.02 ± 0.74	0.0083
PVA/10%MFC	91.39 ± 1.59	0.335 ± 0.0660	32.83 ± 1.67	0.650

this phenomenon can be responsible for the further decrease in surface tension and contact angle, as observed.

Viscosimetry

The rheology of PVA aqueous solutions depends on several factors such as temperature, PVA concentration, percentage of hydrolysis and degree of polymerisation.²⁷ Nevertheless, degree of polymerisation and concentration have been reported as having the stronger effect on the viscosity.²⁸ The reason is that the chain length or the higher chain concentration promotes in larger extent the formation of inter- and intramolecular hydrogen bonding. As a result, water becomes a poorer solvent, and hence, the viscosity of the solution increases. Several authors have

reported the rheological behaviour of PVA solution as shear thinning. The PVA solution analysed in this work ($0.02\ g\ mL^{-1}$) showed basically Newtonian behaviour in a shear rate range from 0 to $400\ 1\ s^{-1}$ (Fig. 6a). Experimental data are in fact well fitted by a linear function ($m = 0.0043$, $R^2 = 0.999$). This means that, for such concentration, inter- and intramolecular interactions are not sufficient to determine a consistent increase in viscosity. The PVA/5%MFC solution showed shear thinning behaviour from 0 up to $80\ 1\ s^{-1}$. Data in this range are well fitted by the Herschel–Bulkely model ($\tau_0 = 0.0139$, $K = 0.0416$, $n = 0.7082$). Beyond $80\ 1\ s^{-1}$, the solution has rather Newtonian behaviour and can be accurately fitted by a linear function having $m = 0.0083$ (Fig. 6b). This suggests



4 Variation of stress versus shear rate for PVA, PVA/5%MFC and PVA/10%MFC at 25°C

that as the shear rate reaches 80 l s^{-1} , structural rearrangement takes place. The PVA/10 MFC solution exhibited analogous behaviour, being fitted by the Herschel-Bulkely model from 0 to 110 l s^{-1} ($\tau_0 = 0.0759$, $K = 0.0670$, $n = 0.6844$) and from 110 l s^{-1} onwards by a linear function having $m = 0.650$ (Fig. 6c). The addition of MFC, therefore, resulted in an increase in viscosity as expected. Cellulose fibres in fact act as a thickener in aqueous solution because of their hydrophilicity.²⁹

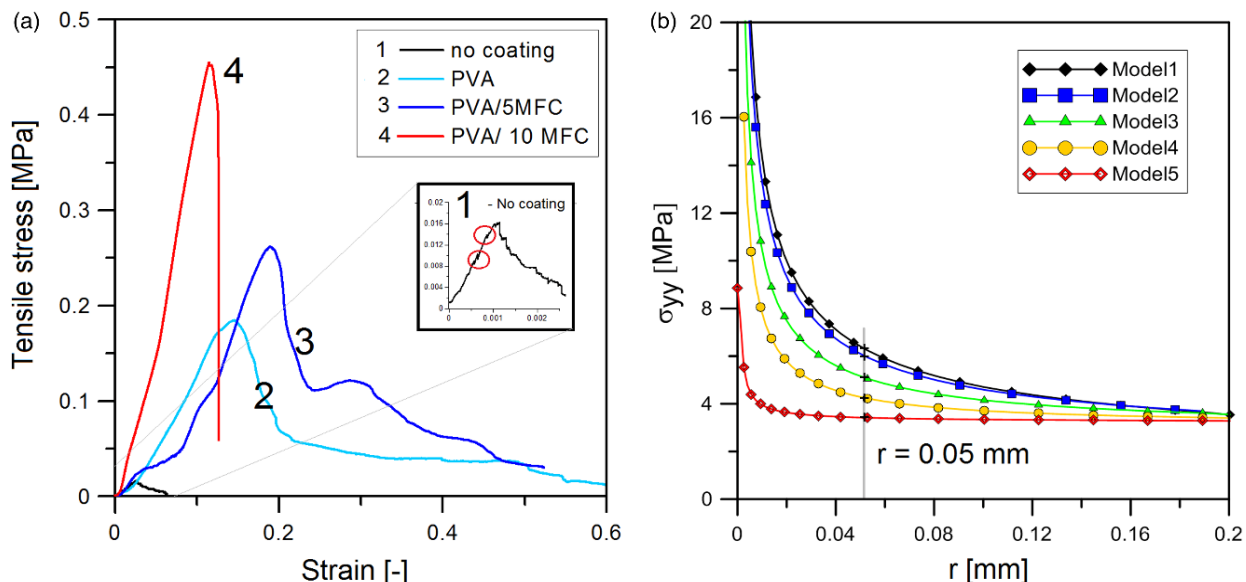
Tensile test

The significant improvement of mechanical properties (strength, strain to fracture and apparent fracture energy) of coated samples can be observed by examining the stress-strain curves obtained from tensile tests (Fig. 5a). In the case of non-coated samples, the increase in load causes fracture of first suitably oriented struts,³⁰ which corresponds to the pop-ins indicated by circles in Fig. 6a. All coated samples do not exhibit any pop-in peaks at the initial stage of load, and the first fracture events take place only at remarkably higher load in comparison with the non-coated samples. The extension of the elastic region and the stress peak σ_t increase with the increasing amount of MFC. Although the FEA was based on a single strut, these outputs, together with contact angle and viscosity measurements, can offer a good interpretation of the tensile results. In fact, previous works confirmed that the mechanical properties of the constituting struts determine the

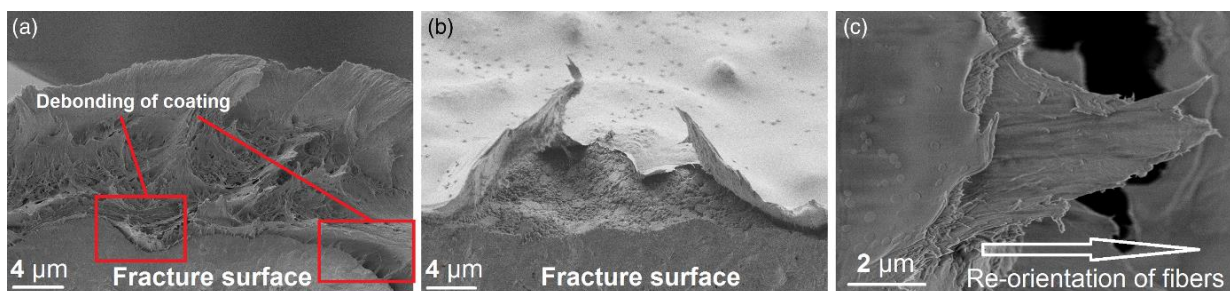
mechanical behaviour of the whole foam.³¹ By considering that MFC has been proven to enhance the infiltration of coating into cracks and that the latter is the main criteria for the reduction of K_I , it can be stated that the experimental results are in good agreement with computed values. In Fig. 5b, the variation of $\sigma_{yy}(r)$ at ($y = 0$) is plotted for models 1–5. The measured contact angles, viscosities, porosity and tensile strength are correlated and summarised in Table 2. The extension of the plateau region decreases with the increasing amount of MFC, indicating a lower elongation capability of PVA/MFC composites, in comparison with neat PVA. A drastic reduction of strain to failure has been in fact reported for MFC reinforced polymer as the percolation concentration is reached.³²

Scanning electron microscopy

Images (SEM) give insights about the quality of the adhesion between coating and scaffolds. Although it is hard to determine whether the presence of MFC enhanced or not the infiltration into surface cracks, it is possible to state that the adhesion of the coating is sufficient in order to transfer the load from the strut to the coating. In Fig. 6a, a detail of a broken strut is shown. The coating appears as strained by tensile stresses; the fracture surface looks like fibrous and characterised by the presence of a multitude of fibres protruded out of the PVA matrix. Moreover, on the right corner, the starting of debonding process can be



5 a characteristic stress versus strain curves from tensile test for non-coated, PVA coated, PVA/5%MFC coated and PVA/10%MFC coated samples and b σ_{22} as function of distance of crack tip ($y = 0$)



6 Details of a, b fracture surfaces of coated struts and c strained coating

detected. This process is better visible in Fig. 6b. In Fig. 6c, the detail of a fractured film is shown. It is possible to observe the MFC fibres embedded into the PVA matrix and aligned along the straining direction.

Conclusions

This work provided new insights to the mechanical behaviour of polymer coated Bioglass® scaffolds. Results from FEM demonstrated that the dominant criterion for the sake of strengthening is the extent of coating infiltration into surface cracks, which is maximised as the polymer reaches the crack tip. As PVA reaches the crack tip, the highest reduction of K_I and σ_{yy} is achieved. It is therefore crucial to optimise the wettability and viscosity of polymeric solutions designed for dip coating (i.e. the choice of a suitable polymer-solvent system and polymer concentration) in order to maximise the infiltration capability into the surface defects. Contact angle measurements of PVA aqueous solutions with different amounts of MFC on Bioglass® surfaces were carried out, showing that the addition of MFC leads to the decrease in contact angle towards the Bioglass® surface, therefore leading to a better wettability. On the other hand, the presence of fibres determines a consistent increase in viscosity in the system. A balance between these two effects must be achieved. Results from tensile tests conducted on uncoated and coated scaffolds were in agreement with the FEM results.

Observations by SEM revealed a homogeneous distribution of the coating on the struts surface and a sufficiently strong interface to guarantee stress transfer from the struts to the coating.

Acknowledgements

Financial support from GlaCERCo-ITN EU project, contract no. 264526, within Marie Curie Action ‘Initial Training Networks’ is acknowledged. Support to this research through the infrastructure project no. ED1.1.00/02.0068 is also acknowledged.

References

1. A. Philippart, A. R. Boccaccini, C. Fleck, D. W. Schubert and J. A. Roether: ‘Toughening and functionalization of bioactive ceramic and glass bone scaffolds by biopolymer coatings and infiltration – a review of the last 5 years’, *Expert Rev. Med. Devices*, 2015, **12**, (1), 93–111.
2. D. M. Yunos, O. Bretcanu and A. R. Boccaccini: ‘Polymer-bioceramic composites for tissue engineering scaffolds’, *J. Mater. Sci.*, 2008, **43**, (13), 4433–4442.
3. G. Yang, X. Yang, L. Zhang, M. Lin, X. Sun, X. Chen and Z. Gou: ‘Counterionic biopolymers-reinforced bioactive glass scaffolds with improved mechanical properties in wet state’, *Mater. Lett.*, 2012, **75**, (15), 80–83.
4. M. Peroglio, L. Gremillard, J. Chevalier, L. Chazeau, C. Gauthier and T. Hamaide: ‘Toughening of bio-ceramic scaffolds by polymer coating’, *J. Eur. Ceram. Soc.*, 2007, **27**, (7), 2679–2685.

5. F. J. Martínez-Vázquez, A. Pajares, F. Guiberteau and P. Miranda: 'Effect of polymer infiltration on the flexural behavior of β -tricalcium phosphate robocast scaffolds', *Materials*, 2014, **7**, 4001–4018.
6. M. Scheffler and P. Colombo: 'Cellular ceramics: structure, manufacturing, properties and applications', 2005, Weinheim, Wiley.
7. L. E. Scriven: 'Physics and applications of DIP coating and spin coating', *MRS Proc.*, PROC-121-717, 1988, **121**.
8. V. G. Levich: 'Physicochemical hydrodynamics', 1962, Englewood Cliffs, NJ, Prentice Hall.
9. B. V. Derjagun and S. N. Levi: 'Film coating theory', 1964, London, Focal Press.
10. H. Snoeijer and B. Andreotti: 'A microscopic view on contact angle selection', *Phys. Fluids*, 2008, **20**, 057101.
11. J. J. Blaker, V. Maquet, A. R. Boccaccini, R. Jérôme and A. Bismarck: 'Wetting of bioactive glass surfaces by poly(α -hydroxyacid) melts: interaction between Bioglass® and biodegradable polymers', *e-Polymers*, 2005, **23**, 1–23.
12. L. Bertolla, I. Dlouhý, A. R. Boccaccini and A. Philippart: 'Mechanical reinforcement of Bioglass®-based scaffolds by novel polyvinyl-alcohol/microfibrillated cellulose composite coating', *Mater. Lett.*, **118**, 204–207.
13. L. L. Bertolla, I. Dlouhý and A. R. Boccaccini: 'Preparation and characterization of Bioglass®-based scaffolds reinforced by polyvinyl alcohol/microfibrillated cellulose composite coating', *J. Eur. Ceram. Soc.*, 2014, **34**, (14), 3379–3387.
14. D. A. White and J. A. Tallmadge: 'A gravity corrected theory for cylinder withdrawal', *AIChE J.*, 1967, **13**, (4), 745–750.
15. A. R. Swenson, S. K. Nicol and A. numerical: 'treatment of the restricted withdrawal of vertical cylinders from quiescent liquids', *J. Colloids Interface Sci.*, 1977, **60**, (3), 568–569.
16. Q. Z. Chen, I. D. Thompson and A. R. Boccaccini: '45S5 Bioglass®-derived glass-ceramic scaffolds for bone tissue engineering', *Biomaterials*, 2006, **27**, 2414–2425.
17. L. L. Hench: 'The story of Bioglass®', *J. Mater. Sci.: Mater. Med.*, 2006, **17**, 967–978.
18. A. J. Svagan, A. S. My, A. Samir and L. A. Berglund: 'Biomimetic polysaccharide nanocomposites of high cellulose content and high toughness', *Biomacromolecules*, 2007, **8**, 2556–2563.
19. 'Adhesives. Wettability. Determination by measurement of contact angle and surface free energy of solid surface', BS EN 828:2013, BSI, London, UK; 2013.
20. 'Advanced technical ceramics – mechanical properties of monolithic ceramics at room temperature. Part 2: determination of Young's modulus, shear modulus and Poisson's ratio', BS ENV 843-2, BSI, London, UK; 2006.
21. A. K. Srivastava, R. Pyare and S. P. Singh: 'Elastic properties of substituted 45S5 bioactive glasses and glass-ceramics', *Int. J. Sci. Eng. Res.*, 2012, **3**, (2), 12.
22. M. I. Baker, S. P. Walsh, Z. Schwartz and B. D. Boyan: 'A review of polyvinyl alcohol and its uses in cartilage and orthopedic applications', *J. Biomed. Mater. Res. B*, 2012, **100**, (5), 1471–1477.
23. F. Chen, D. -J. Kang and J. -H. Park: 'New measurement method of Poisson's ratio of PVA hydrogels using an optical flow analysis for a digital imaging system', *Meas. Sci. Technol.*, 2013, **24**, 055602.
24. T. L. Anderson: 'Fracture mechanics, fundamentals and applications', 3rd edn; 2005, Boca Raton, FL, Taylor and Francis Group.
25. L. Hench: 'Bioceramics', *J. Am. Cer. Soc.*, 1988, **81**, (7), 1705–1728.
26. A. Bhattacharya and P. Ray: 'Studies on surface tension of poly(vinyl alcohol): effect of concentration, temperature, and addition of chaotropic agents', *J. Appl. Polym. Sci.*, 2004, **93**, 122–130.
27. M. Masuda: 'Polyvinyl alcohol-development', 1991, New York, Wiley.
28. B. Briscoe, P. Luckham and S. Zhu: 'The effects of hydrogen bonding upon the viscosity of aqueous poly(vinyl alcohol) solutions', *Polymer*, 2000, **41**, 3851–3860.
29. S. Shafiei-Sabet, W. Y. Hamad and S. G. Hatzikiriakos: 'Rheology of nanocrystalline cellulose aqueous suspensions', *Langmuir*, 2012, **28**, (49), 17124–17133.
30. L. Řehorek, I. Dlouhý and Z. Chlup: 'Tensile behaviour of open cell ceramic flaks', *Ceramics – Silikáty*, 2009, **53**, (4), 237–241.
31. R. Brezny, D. J. Green and C. Q. Dam: 'Evaluation of strut strength in open-cell ceramics', *J. Am. Ceram. Soc.*, 1989, **72**, (6), 885–889.
32. T. Zimmermann, E. Pöhler and T. Geiger: 'Cellulose fibrils for polymer reinforcement', *Adv. Eng. Mater.*, 2004, **2**, 754–761.